



Determining the critical blasting load of cracked strip bauxite pillars

Li-chun Jiang^{1,2} · Bin-bin Shen² · Luan-luan Xue³

Received: 1 June 2020 / Accepted: 22 March 2021 / Published online: 1 April 2021
© Springer-Verlag GmbH Germany, part of Springer Nature 2021

Abstract

Cracked pillars have limited capabilities for the bearing of dynamic and static loads, consequently threatening the stability of entire goafs. In the current study, we establish a structural mechanical model for cracked strip pillars and determine a mathematical formula for the total energy based on an underground bauxite mine in Shanxi, China. Furthermore, the instability criterion is employed to derive an analytical method for the estimation of the critical blasting load q_{cr} for cracked strip bauxite pillars. The relationship between q_{cr} and pillar height (H), pillar width (b), pillar length (L), and the crack loosen zone width (d) is quantitatively evaluated. Results demonstrate that when L and d are constant, q_{cr} decreases as H increases. Moreover, q_{cr} is observed to increase with b for constant H and d , with a continuous reduction in curvature fluctuations. Although q_{cr} increases with L for fixed H and b , the increase amplitude is small, indicating the limited influence of L . For constant L and b , q_{cr} decreases as d increases, and when the value of d exceeds that of the inflection point, the rate of change is steeper. The proposed analytical method is validated using numerical results and a case study. Our work provides theoretical support for the safe production of bauxite mining.

Keywords Pillar · Mechanical model · Critical blasting load · Crack loosen zone · Sedimentary bauxite

Introduction

The sedimentary bauxite deposits in Shanxi, China, are generally layered in a stratoid form, with a large (several km²) and narrow (less than 3.0 m) mining area and an obscure boundary between the orebody and surrounding rock strata. Strip open stope mining is the most commonly used method for the underground mining of this type of deposit (Lin 2017), with a protective roof of specific thickness and strip pillars of specific width to form a goaf support system. Internal joint development and damage from mining can result in the frequent cracking of reserved strip pillars, making them structurally defective (Nazarov et al. 2014). In particular, when the internal accumulated energy of the pillar exceeds the ultimate bearing threshold under an overburdening rock mass and far-field

blasting stress wave, the cracked pillar is likely to collapse and lose stability, consequently leading to the collapse of entire goafs group (Abdellah et al. 2014; Zhao et al. 2016; Jiang et al. 2017a; Huang et al. 2019). Therefore, determining the critical blasting load for cracked strip bauxite pillars is crucial in order to avoid any unexpected failures of the pillar as well as the surrounding rock strata and also reduces the probability of accidents within bauxite mines.

Strip pillars in underground bauxite mines act as a natural support for the overlying strata, ensuring the safety of both operators and equipment. Numerous studies have investigated the stability of pillars, making substantial theoretical progress. For example, the loads, strength, instability potential function, and failure form of pillars were evaluated in order to determine eight key influencing factors for the stability of rectangular pillars, and a simplified mathematical formula was proposed to calculate the corresponding safety factors (Yin et al. 2012). Moreover, the coal mining depth and nature of fractured rock mass in collapse zones were employed to calculate the ultimate strength of pillars (Singh et al. 1996, 2011). Sellers and Klerck (2000) conducted a series of physical and numerical model tests to describe the crack propagation process inside the rock mass of pillars under high confining pressures. Swift and Reddish (2002) empirically investigated the safety of roof beams and pillar failure associated with a shallow room and

✉ Luan-luan Xue
xueluanluan@scut.edu.cn

¹ School of Civil Engineering and Transportation, South China University of Technology, Guangzhou 510640, China

² Institute of Safety Science and Engineering, South China University of Technology, Guangzhou 510640, China

³ State Key Laboratory of Subtropical Building Science, South China University of Technology, Guangzhou 510640, China

pillar ironstone mine in detail using empirical approaches. Yang et al. (2015a) investigated the effect of a multi-gob, pier-type roof structure on coal pillar load-bearing capacity. Idris et al. (2015) proposed a random evaluation method for the stability of pillars based on artificial neural networks. Shi et al. (2017) investigated the failure width of banded pillars based on the composite crack failure mode via a calculation model of pillar failure width.

The mining process results in static and dynamic impact loads (blasting operations), which can result in further crack propagations and pillar failure, subsequently leading to the collapse of the goaf. Kutuzov and Tyupin (2017) proposed a theoretical formula to determine the blast hole spacing and delay interval using the energy dissipation principle to analyze the stress state of blasting operations that have an effect on jointed pillars. Deng et al. (2019) used numerical methods to simulate the failure process of pillars triggered by dynamic disturbances under different lateral pressure coefficients and revealed the dynamic buckling mechanism of rock burst for pillars. Li et al. (2019) investigated the rock burst buckling instability of strip pillars in terms of static stress and loading disturbance, with a focus on the dynamic criterion of pillar instability based on the dynamic and static energy index. Planinc and Schnabl (2019) proposed an analytical solution for the critical buckling loads of compressed columns by considering the effects of simultaneous transverse cracking and longitudinal delamination. Lu et al. (2017) proposed an instability evolution model for pillars in the mining of multi-middle orebody in order to investigate the crack instability evolution law of hard rock pillars under multiple excavation disturbances. Yugo and Shin (2015) employed numerical simulations to study the effect of blasting operations from adjacent stopes on the stability of strip pillars. Agrawal and Mishra (2019) summarized the vibration effects resulting from blasting using an improved scale distance regression analysis method.

However, despite the progress made by the aforementioned studies, the influence of blasting stress waves on the behavior of bauxite pillars and the instability of cracked strip bauxite pillars are rarely considered. In particular, the crack propagation within the pillar under dynamic disturbances is generally ignored, resulting in errors in the pillar strength calculations.

In order to overcome the lack of an available strength formula for cracked strip bauxite pillars, we evaluate the stability of defective strip bauxite pillars by determining the critical blasting load. This is performed using an analytical approach that can be conveniently adopted in practical engineering applications. In particular, we first establish a mechanical model for cracked strip bauxite pillars based on a case study of a sedimentary bauxite underground mine in Shanxi, China. Following this, the analytical solution of the critical blasting load for cracked strip

bauxite pillars is developed using the energy dissipation principle (Chen et al. 2012), considering the influence of the internal crack propagation loosen zone. The proposed critical blasting load formula is applied to evaluate the instability conditions of cracked pillars and to quantitatively study the relationship among the critical blasting load, pillar height, length, width, and the crack loosen zone width. The derived critical blasting load formula is validated through numerical results and engineering monitoring data.

Mechanical model of cracked strip pillar

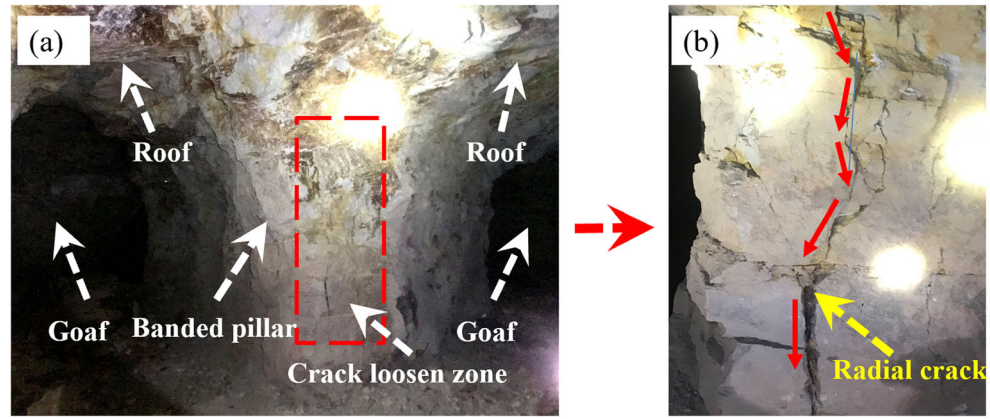
Mechanical model

Based on field investigations of the exploration of the Chenguang underground bauxite mine, located at Liulin County in Shanxi, China, we found macroscopic cracks to appear at the edge of the pillar during mining, where the rock blocks peel off are removed by the required equipment. The further development of the radial cracks inside the pillar directly affects the bearing capacity of the strip pillar. Therefore, this study mainly focuses on the radial propagation cracks inside the pillar. We target goaf 3#, located within the middle production +1160 m of the mine (Fig. 1). Figure 2a presents a schematic diagram of the proposed structural model of the pillar. The central area of the pillar is assumed to contain radial cracks, presented with “Type I” tensile propagation, and the surrounding area of the radial cracks is defined as a loosen zone with crack enrichment. The cross-section stress analysis of the pillar is demonstrated in Fig. 2b, where self-stress P_0 of the overlying rock (soil) strata uniformly acts on the top of the pillar, and the blasting stress wave of the adjacent stope directly acts on the free sidewall of the pillar. H , L , b , and d are the pillar height (m), length (m), width (m), and crack loosen zone width (m), respectively.

A large friction force F_t exists between the pillar and the overburden rock strata (Fig. 2a) (Yang et al. 2015b); thus, the horizontal displacement of the contact surface between the pillar top and the surrounding rock strata is relatively small under overburden stress P_0 , and consequently, no large displacement deformation occurs. The pillar experiences drum-shaped (Poisson) splitting expansion deformation (Xia et al. 2017) and radial cracks are induced in the central area of the pillar due to the absence of an effective binding force on the free sidewall of the pillar. The cracks are further extended with the increase in gravity loading time and the influence of frequent blasting disturbances. If the center axis of the bearing loads is altered, the bearing centerline of the pillar will shift.

In order to simplify the calculation of the total potential energy (II) of the cracked strip bauxite pillar, we make the following assumptions.

Fig. 1 Images of field site. (a) Mining area. (b) Pillar with radial crack



- (1) The rock mass of the strip pillar is assumed to behave continuously and elastically with a complete internal structure. Only the influence of radial crack propagation is considered, while the influence of lateral cracks is ignored because there is no horizontal sliding failure of pillar.
- (2) The internal displacement and deformation of the strip pillar are infinitesimal, that is, the displacement amplitude of the internal media in the rock mass is much smaller than the macro deformation value of the pillar. For the analysis of the potential energy, only the elastic deformation is considered, and the plastic deformation is ignored.
- (3) The blasting stress acts uniformly on the free longitudinal section of the strip pillar along the horizontal direction.

Total potential energy of cracked strip pillar

Due to a severe water shortage, there are no filling conditions at the Shanxi underground bauxite mines, and thus no filling operations are carried out in the goaf. The elastic strain energy of the pillar and the dissipated energy of the crack loosen zone are generally derived from the energy converted from the work done by overlying rock (soil) gravity P_0 and blasting stress q_d . Therefore, the total potential energy of the cracked strip pillar is largely composed of the strain potential energy U_w generated by the deflection deformation of the pillar, the gravity potential energy U_k of the pillar, the elastic potential energy of the strain accumulation U_v from the fractured rock mass, and the work done by external loads W .

We initially determine the analytical formulae of the aforementioned potential energies. Following this, the expression

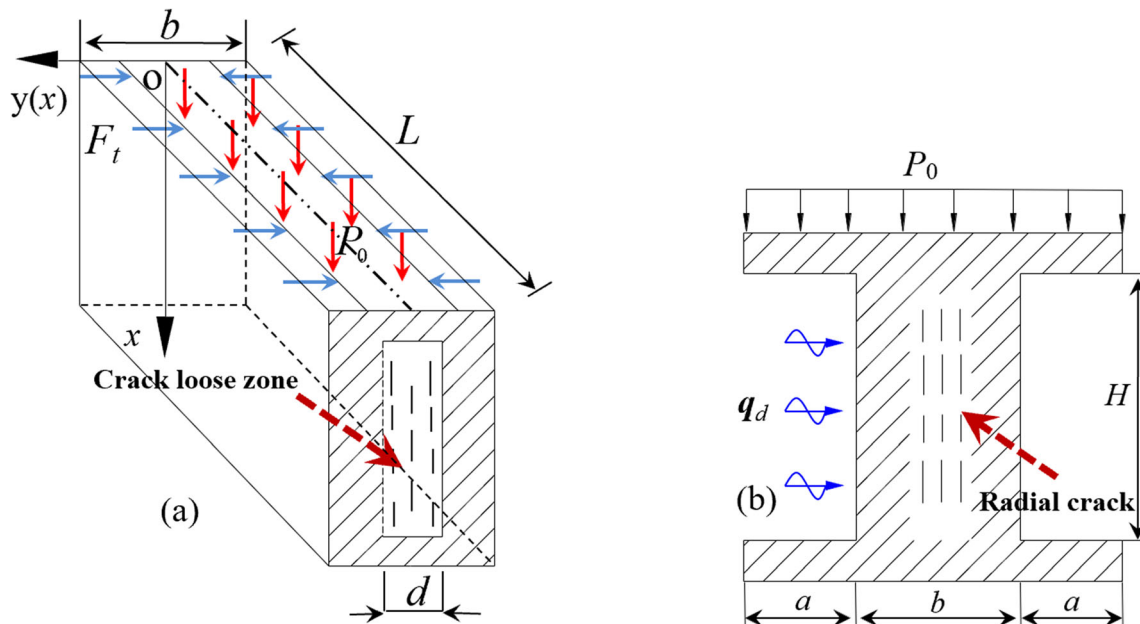


Fig. 2 Proposed mechanical model of cracked strip pillar. (a) Structural model. (b) Stress analysis of cross section

of total potential energy Π of the cracked strip pillar is derived under multiple force coupling based on the principle of energy superposition. This process is detailed in the following.

1. Strain potential energy U_w of pillar

The strip pillar is regarded as a thick spatial structure plate with radial support. The y - x coordinate system for the strip pillar is shown in Fig. 2. According to the failure mode and the boundary conditions of a thick plate (Zhou et al. 2016), the deflection can be expressed as follows:

$$y = A \left(1 - \cos \frac{2\pi x}{H} \right) + B \left(1 - \cos \frac{6\pi x}{H} \right) \tag{1}$$

where A and B are the deflection coefficients in the x and y directions, respectively.

Furthermore, the bending strain potential energy U_w of the pillar can be described as:

$$U_w = \frac{1}{2} \int_0^H \frac{M(x)^2}{EI} ds = \frac{EI}{2} \int_0^H (y')^2 ds \tag{2}$$

where E is the elastic modulus of the pillar rock mass, I is the inertia moment of the strip pillar, $M(x)$ is the bending moment at the height of x , and d_s is the end arc length of the strip pillar bending deformation, with $ds = \sqrt{1 + (y')^2} dx$.

We expand ds via the Taylor series in order to simplify bending strain potential U_w by omitting the first (y') and second (y'') order small values:

$$U_w = \frac{\pi^4 (A^2 + 81B^2) Eb}{3} \tag{3}$$

The gravity potential energy U_k of the pillar is expressed as (Xu et al. 2017):

$$U_k = 0.5mgH = 0.5\rho gLbH^2 \tag{4}$$

where ρ is the density of the orebody and g is the acceleration of gravity.

2. Elastic potential energy U_v of crack loosen zone

The long-term action of overburden rock mass (soil) P_0 generally leads to the dilatancy deformation of the rock mass in the central area of the pillar, which further leads to radial cracks, and part of the elastic potential energy resulting from the bulk strain will be accumulated. According to the minimal energy principle for the dynamic failure of rock mass (Zhao et al. 2003), the minimum energy U_{\min} required for pillar failure is:

$$U_{\min} = \frac{\sigma^2}{2E} \tag{5}$$

where σ is the uniaxial compressive strength of the orebody.

In practical engineering applications, the energy required for pillar failure is far greater than U_{\min} owing to the coupling effect of multiple forces. The safety factor k ($k > 1$) is introduced to represent the influence of multiple force coupling. The area of maximum spacing between the radial cracks is defined as the crack loosen zone, with a width of d . The general integral form of the strain elastic potential energy of the crack loosen zone can be written as follows:

$$U_v = \int k U_{\min} \frac{bL^2}{d} dx = \frac{k\sigma^2 bL^2 H}{2Ed} \tag{6}$$

3. External work W

Figure 3 demonstrates the simplified displacement mechanical model of the pillar, where the red arc area represents the fictitious deformation zone of the pillar under the action of

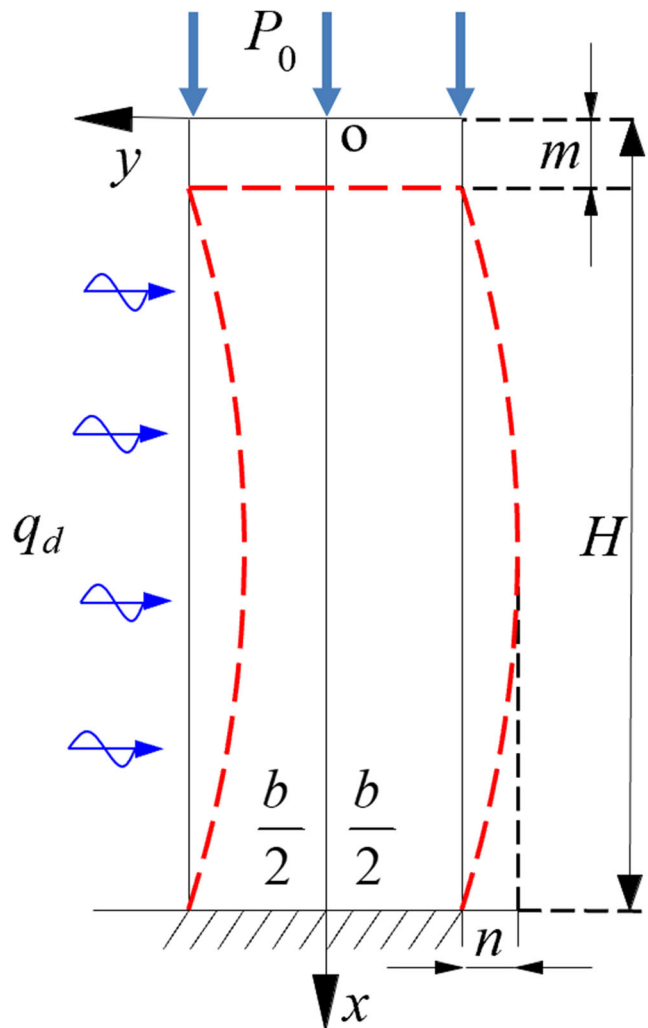


Fig. 3 Simplified displacement mechanical model of the pillar

P_0 and q_d , m is the radial generalized displacement corresponding to P_0 , and n is the lateral generalized displacement corresponding to q_d .

Using the energy relationship (Chen et al. 2015), the work W_{P_0} and W_{q_d} done by the overburden stress and blasting stress can be expressed, respectively, as follows:

$$\begin{cases} W_{P_0} = P_0 m \\ W_{q_d} = q_d n \end{cases} \quad (7)$$

where $m = \frac{1}{2} \int_0^H (y')^2 dx$, which can be substituted into Eq. (7). The general solution is:

$$\begin{cases} W_{P_0} = P_0 m = \frac{\pi^2 (A^2 + 9B^2) P_0}{H} \\ W_{q_d} = q_d n = (1 + B^2) q_d H^2 L \end{cases} \quad (8)$$

4. Total potential energy II of cracked strip pillar

Thus, based on the energy superposition principle, the total potential energy II of the cracked strip pillar can be derived as follows:

$$\begin{aligned} II = U_w + U_k + U_v - W_{P_0} - W_{q_d} = & \frac{\pi^4 (A^2 + 81B^2) Eb}{3} \\ & + 0.5 \rho g b L H^2 + \frac{k \sigma^2 b L^2 H}{2Ed} - (1 + B^2) q_d L H^2 - \frac{\pi^2 (A^2 + 9B^2) P_0}{H} \end{aligned} \quad (9)$$

Critical blasting load

Instability criterion

From the energy dissipation principle (Li et al. 2016), when $II'' > 0$ ($II'' < 0$), the cracked strip pillar is stable (unstable), and when $II'' = 0$, the cracked strip pillar is in a critical state.

When the cracked strip bauxite pillar is exposed to the stresses of overburden rock mass and blasting load, the potential energy function of the pillar is minimized. Furthermore, when the blasting load reaches a certain limit, the tensile stress will concentrate around the free surface of the pillar. In order to avoid the instability and destruction of the pillar, the total potential energy of the strip pillar should satisfy $II'' \geq 0$.

Critical blasting load

Both static and dynamic loads affect the stability of pillars (Wang and Li 2010). As static loads are relatively constant, we focus on the blasting dynamic load in order to meet the

calculation requirements for the dynamic stability of cracked pillars.

By expressing $II = 0$, the blasting stress can be calculated as follows:

$$q_d = \frac{\pi^4 (A^2 + 81B^2) Eb}{3(1 + B^2) L H^2} + \frac{\rho g b}{2(1 + B^2)} + \frac{k \sigma^2 b L}{2(1 + B^2) Ed H} - \frac{\pi^2 (A^2 + 9B^2) P_0}{(1 + B^2) L H^3} \quad (10)$$

Moreover, we apply the catastrophe theory of non-linear science (Qin et al. 2001) to determine the steady-state equation of the strip pillar as:

$$\begin{cases} \frac{\partial II}{\partial A} = 0 \\ \frac{\partial II}{\partial B} = 0 \end{cases} \quad (11)$$

Substituting Eqs. (9) and (10) into (11), the solution is obtained as follows:

$$\begin{cases} B = 0 \\ q_d = \frac{27 \pi^4 Eb H - 9 \pi^2 P_0}{L H^3} \end{cases} \quad (12)$$

Setting A and B as state variables, we solve the first derivative of the total potential energy II' and then set the solution to zero in order to solve the equilibrium surface equation of the strip pillar system. The two state variables in the total potential energy equation result in two sharp points on the equilibrium surface. From the energy catastrophe theory, the sharp point on the equilibrium surface corresponds to $II'' = 0$, indicating the critical state of the strip pillar at this time. Due to the smoothness of the equilibrium surface, II'' at the sharp point can be described as follows:

$$\begin{cases} \frac{\partial II}{\partial B \partial B} = 54 \pi^4 Eb - 2 q_d L H^2 \frac{18 \pi^2 P_0}{H} = 0 \\ \frac{\partial II}{\partial A \partial A} = 0 \end{cases} \quad (13)$$

Therefore, when $B = 0$, the sharp point on the equilibrium surface corresponds to $II'' = 0$, that is, when $B = 0$, the potential function II of the cracked strip bauxite pillar is minimized, and the cracked strip pillar is in a critical state. By substituting $B = 0$ into Eq. (10), we can solve the critical blasting load q_{cr} (Mpa) as follows:

$$q_{cr} = \frac{\pi^4 A^2 Eb}{3 L H^2} + \frac{\rho g b}{2} + \frac{k \sigma^2 b L}{2 Ed H} - \frac{\pi^2 A^2 P_0}{L H^3} \quad (14)$$

In Eq. (14), E (Mpa), P_0 (N), A , and k are kept constant for the strip pillar. Therefore, the principle factors affecting the critical blasting load of the cracked strip pillar are pillar height H , width b , length L , and width d of the crack loosen zone.

In practical underground engineering applications, the height, width, and length of the pillars are controllable variables, while the width of the crack loosen zone is non-controllable.

Influencing factors

The complexity of underground mine engineering makes it difficult to accurately control the explosive equivalent of each blasting. Following a blasting operation, a large number of long- and wide-scale cracks often appear inside the pillar. This seriously reduces the overall strength of the pillars and can lead to their eventual collapse. Therefore, research on the quantitative relationship between the critical blasting load and pillar height (H), width (b), length (L), and the crack loosen zone width (d) can provide a theoretical basis for the stability analysis of cracked strip pillars.

General conditions

Data was collected from the Chenguang underground bauxite mine located in the Lvliang Mountains and the western edge of the Loess Plateau at Liulin County in Shanxi, China (Fig. 4a). The geographic distribution of the mine is $37^{\circ} 26' 43''$ – $37^{\circ} 27' 26''$ N and $110^{\circ} 54' 29''$ – $110^{\circ} 54' 51''$ E. The bauxite orebody is situated on the Ordovician erosion surface and the lower part of the Benxi formation in the Carboniferous Middle System. The deposit generally exhibits a bedded and stratoid form, with an average thickness of less than 5.0 m and a general strike of approximately 33° northeast. Furthermore, it is inclined to the northwest direction, with a dip angle within 5.0° – 12.0° and an average dip angle less than 10.0° . The surface is characterized by gullies, the terrain is deeply cut, and the weathering and denudation are strong (Fig. 4b). There is no fault and collapse column in the mining area, and the geological structure is simple. From the top to the bottom layer, the overburden rock (soil) strata largely consist of loess, metasandstone, slate, and Shanxi-type hard clay. The hardness coefficient f of the bauxite lies between 8.0 and 12.0, and the

joints and fractures in the orebody are well developed. Strip open stope mining is the principle technique applied on the mine, with millisecond short delay blasting using 2 # rock explosives.

Physical and mechanical parameters

The physical and mechanical parameters of the bauxite rock mass are determined according to the geological exploration data and the laboratory experimental data (Fig. 5), as reported in Table 1. The mechanical strength of the rock sample is lower than that of the original rock mass, because the experimental rock sample is carried out after excavation and blasting. A value of 0.0015275 for A denotes the internal force and deflection coefficients taken from Zuo et al. (2014). Based on preliminary testing, we set safety factor k to 1.92. The buried depth of the orebody is 120.0 m, and the self-weight stress of the surrounding rock (soil) strata is $P_0 = 2.70$ Mpa.

Pillar height H

In order to investigate the influence of pillar height on the critical blasting load, the length of the cracked strip pillar ($L = 100.0$ m) and the width of the crack loosen zone ($d = 1.0$ m) were kept constant, and the pillar height (H) was set between 3.0 and 6.0 m. The pillars were divided into three groups according to their width (3.0, 4.0, and 5.0 m). Figure 6 presents the variation of pillar critical blasting load determined from Eq. (14) with respect to height H across pillar widths.

For constant strip pillar length L and crack loosen zone width d , the critical blasting load q_{cr} was observed to decrease as pillar height H increased. This is attributed to the weaker self-stable bearing capacity of the cracked pillar at greater heights. Furthermore, as the width was reduced, the center of gravity of the curve shifted downward and closer to the origin of the coordinate. This indicates that at a fixed height, the narrower the cracked pillar width, the smaller the critical blasting load q_{cr} and the higher the risk of collapse and instability.

Fig. 4 Field site at Chenguang bauxite mine. (a) Geographical location map of the mine. (b) Image of the mine surface





Fig. 5 Compression experiment of the bauxite rock mass

Pillar width *b*

In order to reveal the influence of pillar width on the critical blasting load, the height of the cracked strip pillar (*H*) and the crack loosen zone width (*d*) were fixed at 5.0 and 1.0 m, respectively, and the pillar width (*b*) was set between 3.0 and 5.0 m. The pillars were divided into three groups according to their length (60.0, 80.0, and 100.0 m). Figure 7 presents the variation of pillar critical blasting load determined from Eq. (14) with respect to width *b* across pillar lengths.

Critical blasting load q_{cr} increased with pillar width *b* for constant pillar height *H* and crack loosen zone width *d*, while its variation rate decreased. When the pillar width increased to a certain value (about 5.0 m), the critical blasting load stress value stabilized. This implies that the influence of the internal cracks on the anti-blasting impact ability of the strip pillars was limited for greater widths. Furthermore, as the pillar length decreased, the center of gravity of the curve shifted downward and got closer to the origin of the coordinate. Thus, at a fixed height, the shorter the cracked pillar length, the smaller the critical blasting load q_{cr} and the higher the risk of collapse and instability.

Pillar length *L*

The influence of pillar length on the critical blasting load was evaluated by fixing the height of the cracked strip pillar (*H* = 6.0 m) and the pillar width (*b* = 5.0 m). In addition, the pillar length (*L*) was set between 60.0 and 100.0 m, and the pillars

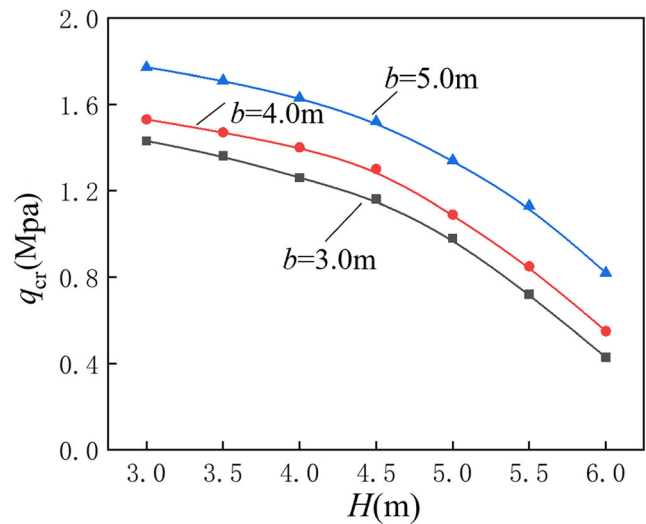


Fig. 6 Variation of critical blasting load q_{cr} with respect to height *H* across pillar widths

were divided into three groups according to their crack loosen zone widths (1.0, 1.2, and 1.4 m). Figure 8 presents the variation of pillar critical blasting load determined from Eq. (14) with respect to length *L* across crack loosen zone widths.

For a fixed strip pillar height (*H*) and width (*b*), the critical blasting load q_{cr} increased with pillar length *L*. Comparing Figs. 6 and 7 demonstrates that the critical blasting load amplitude exhibited minimal variations across pillar length and the influence of pillar length on the critical blasting load was limited. This is a result of the much larger strip pillar length compared to its height and width, while the propagation of the explosion stress wave from the adjacent stope blast source had a fan-like effect, acting on the partial free sidewalls of the strip pillar. Moreover, as the width of the crack loosen zone width increased, the center of gravity of the curve shifted downward, moving closer to the origin of the coordinate. This indicates that for a fixed pillar length, the larger the crack loosen zone width, the smaller the critical blasting load q_{cr} and the higher the risk of collapse and instability.

Width of crack loosen zone *d*

The impact of the crack loosen zone width on the critical blasting load was investigated by fixing the cracked strip pillar length (*L* = 100.0 m) and width (*b* = 5.0 m). Moreover, the crack loosen zone width (*d*) was set within 0.0–2.0 m, and the pillars were divided into three groups according to their height

Table 1 Physical and mechanical parameters of bauxite

Parameters	Volumetric weight ($\gamma/\text{kN}\cdot\text{m}^{-3}$)	Elastic modulus (<i>E</i> /Gpa)	Compressive strength ($[\sigma]/\text{Mpa}$)	Poisson ratio (μ)	Friction angle ($\varphi/^\circ$)	Cohesion (<i>c</i> /Mpa)
Value	22.50	3.50	8.17	0.24	45.52	4.32

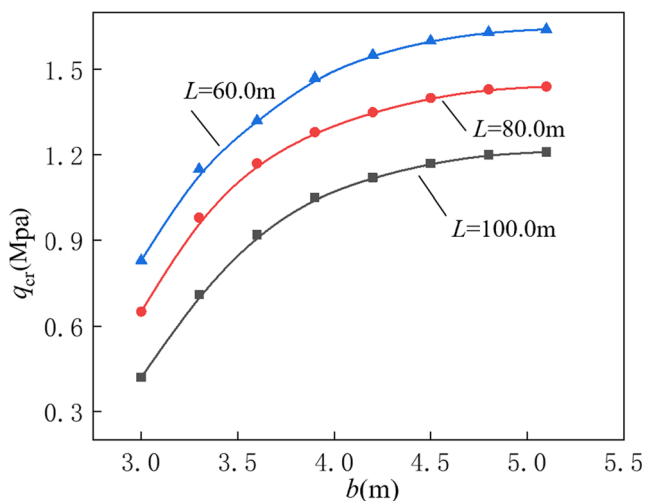


Fig. 7 Variation of critical blasting load q_{cr} with respect to width b across pillar lengths

(4.0, 5.0, and 6.0 m). Figure 9 presents the variation of pillar critical blasting load determined from Eq. (14) with respect to crack loosen zone width d across pillar heights.

For a fixed strip pillar length (L) and width (b), the critical blasting load q_{cr} decreased as crack loosen zone width d increased and was negatively correlated with pillar width b . Furthermore, the curve exhibited an inflection point. There was an obvious increase in the rate of reduction of q_{cr} for values of d greater than the inflection point. This coincides with the degradation of the mechanical performance of the pillar and a rapid reduction in the anti-blasting impact ability.

Figure 9 demonstrates the variation of the critical blasting load q_{cr} with respect to the crack loosen zone width d across pillar heights. There was a downward shift in the center of gravity of the curve as the pillar height increased, which consequently decreased the width d of the loosen zone at the

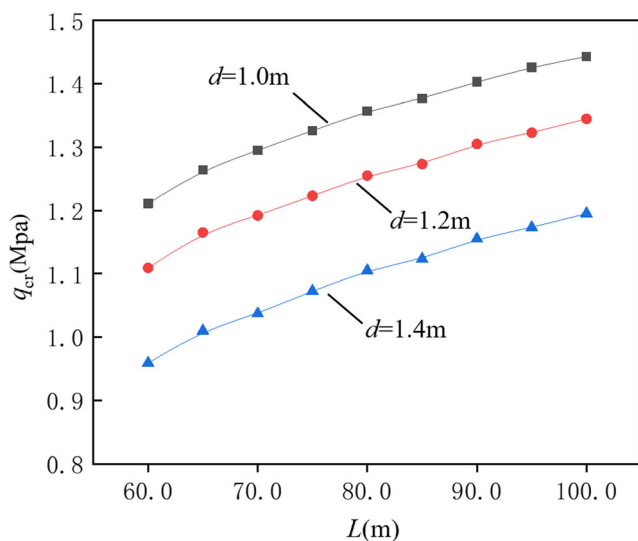


Fig. 8 Variation of critical blasting load q_{cr} with respect to length L across crack loosen zone widths

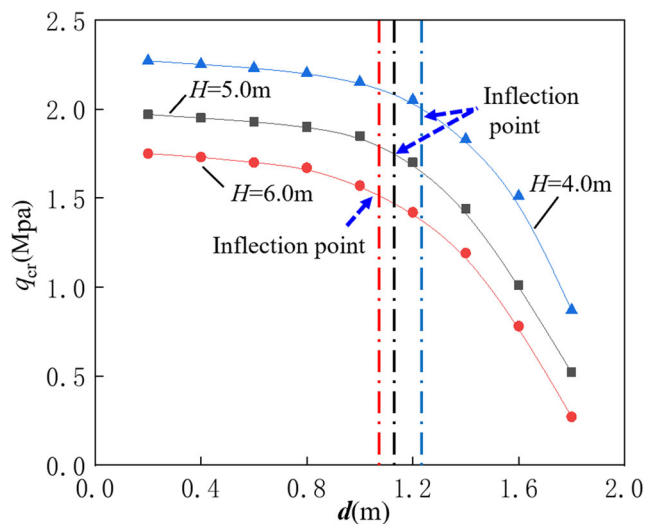


Fig. 9 Variation of critical blasting load q_{cr} with respect to crack loosen zone width d across pillar heights

inflection point. This indicates that for a fixed pillar height, the larger the crack loosen zone width, the greater the degradation damage of the strip pillar. This subsequently corresponds to larger reductions in the critical blasting load stress of the self-steady bearing. In addition, the higher the pillar height, the greater the influence of the crack loosen zone width on the critical blasting load of the cracked strip pillar.

Our results indicate that, in order to ensure the stability of a pillar with radial propagation cracks, each blasting stress must be less than the critical blasting load. For a constant blasting load, measures such as reducing pillar height and pillar length and increasing pillar width can improve the stability of the cracked strip pillars.

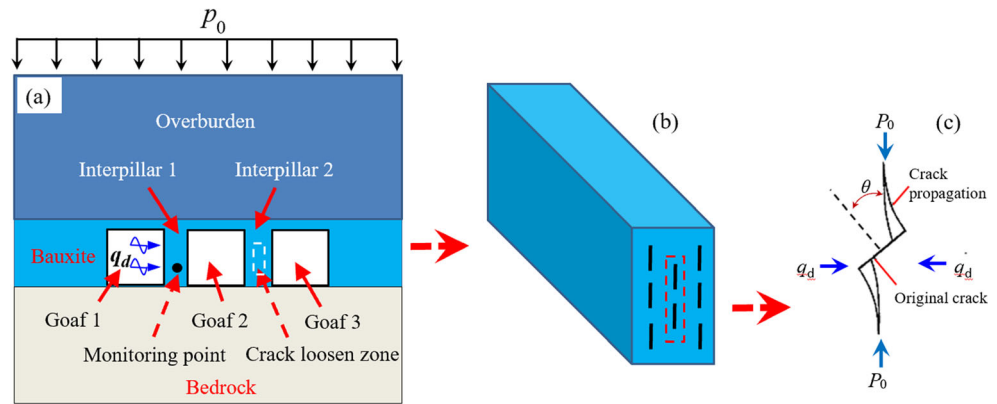
Numerical verification

In order to verify the reliability of the proposed analytical method in determining the critical blasting load q_{cr} for cracked strip bauxite pillars, we performed numerical simulations with three unit goafs (Fig. 10). Midas-GTS/NX 2017 was applied to simulate the excavation of each goaf unit. The influence of dynamic and static loads on the stability of the reserved pillars was considered, allowing for the monitoring of the particle speed change rule inside the pillars. The specifications of the model simulations are described as follows.

(1) Strip pillar parameters

The length and height of the strip pillar were 100.0m and 6.0 m (Fig. 10a), respectively. “Type I” tensile-extended radial cracks were preset inside the pillar, with a crack loosen zone width of 0.7 m (Fig. 10 b and c). The width of the reserved

Fig. 10 Numerical simulation model. (a) Structure of goaf, (b) cracked strip pillar, (c) radial crack propagation



pillar was set as 4.0 m. The physical and mechanical parameters of the bauxite rock mass are reported in Table 1.

(2) External loads

1 The overburden loess thickness was set as 120.0 m, while 2.7 Mpa was used for the self-weight stress, which was directly loaded on the upper contact surface of the pillar roof.

2 The input formula of the blasting stress from the adjacent stopes is described as $q_d(t) = 5000 \sin 10\pi t$ (Jiang et al. 2017b), acting on the cross section of the free sidewall of the pillar (Fig. 10a), where t represents time.

3 Five datasets were used for comparative analysis, including peak values 0.50, 1.00, and 2.00 Mpa. The analytical critical blasting load q_{cr} and maximum blasting load permitted by the safety regulations were considered when determining the parameter values. For example, the proposed analytical critical blasting load of the cracked strip pillar determined from Eq. (14) was 1.35 Mpa, and according to the Blasting Safety Regulations (GB6722-2014) (2015), the maximum allowable blasting load of the pillar was 1.42 Mpa.

- (3) Boundary setting and failure criteria. The viscoelastic damping boundary was set on the four sides of the model, while the free and fixed boundaries were set at the top and bottom of the model, respectively. The failure of the rock mass followed the Mohr-Coulomb criterion.
- (4) The monitoring position was located at pillar No. 1 (Fig. 10a).
- (5) Result and discussion. Figure 11 shows the velocity response time-history curve of the monitoring point under the blasting loads of 0.50, 1.00, 2.00, 1.35, and 1.42 Mpa.

For blasting dynamic loads of 0.50 and 1.00 Mpa, respectively, the velocity of the monitoring point was much less than the analytical value of the critical blasting load velocity, as well as the maximum permitted value (GB6722-2014)

(2015). This demonstrates the stable state of the pillar. When the blasting load was 2.00 Mpa, the velocity of time-history curve of the monitoring point exceeded 23% of the upper limit of the analytical critical vibration speed and 21.2% of the upper limit of the maximum permitted value. This indicates the possible instability of the pillar. Furthermore, the analytical value of the critical blasting load velocity was less than the maximum permitted value by approximately 4%, indicating the close-to-critical state of the pillar.

The numerical simulation results are generally consistent with the proposed analytical results, thus verifying the rationality of the analytical method.

Case study

Goaf 3# located within the middle production section +1160 m of the underground bauxite was selected as the object of the case study (Figs. 1 and 12). The stability monitoring of the pillar under long-term dynamic and static loads was performed across the period between April and September 2019. Field measurements determined the goaf span as 4.2 m, the radial crack height as 2.3 m, the crack loosen zone width as 1.18 m, and the strip pillar length, height, and width as 86.4, 5.0, and 4.0 m, respectively (Fig. 1).

In terms of the static load monitoring of the overburden rock (soil) strata, there was no collapse in the goaf within 30 days after the completion of the mining. This suggests that the cracked strip pillar was able to bear the static load of the overburden rock (soil) strata (Figs. 1 and 12).

The Chengdu Zhongke Blasting Vibration Velocity Monitor TC-4850 from the Chinese Academy of Sciences was employed to monitor the impact of blasting stress waves from the adjacent stopes (Fig. 3), with a range of 0.001–35.4 cm/s, resolution of 0.01 cm/s, and reading accuracy of 0.1%. The monitoring point was located on the floor at the lower edge of the pillar in contact with the roadway. The sensor and the rock mass were rigidly fixed.

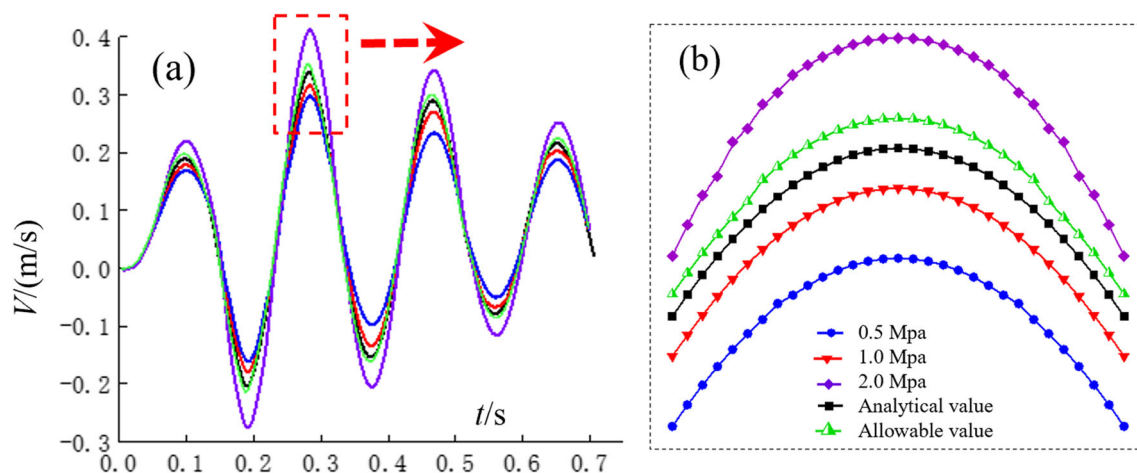


Fig. 11 Velocity-time curve of the monitoring point under different blasting loads. (a) Velocity. (b) Partial enlarged drawing

The non-static millisecond short delay blasting was adopted in the adjacent stopes. The total explosive equivalent of each blasting was 24.0 kg, and the maximum single-stage explosive equivalent was 12.0 kg. The peak vibration velocity resulting from the blasting stress wave at the monitoring point was measured as 0.29 m/s (Fig. 13). Following a conversion based on the Blasting Safety Regulations (GB6722-2014) (2015), the maximum single-stage blasting load was determined as 1.24 Mpa.

The critical blasting load of the pillar was determined as 1.12 Mpa by Eq. (14). In comparison, the actually measured blasting load exceeded 11% of the analytical critical value, that is, exceeded the analytical limit bearing capacity of the cracked strip pillar. This indicates the possible instability of the pillar.

The instability and collapse of the pillar were frequently observed in the target area during the later period of the monitoring time window, and consequently, the goaf was observed to seriously collapse (Fig. 14). This reveals the inability of the cracked pillar to bear the long-term blasting load



Fig. 12 Image of the goaf used in the stability monitoring experiment

beyond the critical value. The experimental results verify the rationality of the proposed analytical method.

Discussion

The analytical solutions of the critical blasting load may exhibit calculation errors as the rock mass of the strip bauxite pillars is not completely continuous and elastic and has non-linear deformation characteristics. In order to improve the analytical calculation accuracy of the critical blasting load for cracked strip bauxite pillars, crack propagation factors can be adopted to perfect the theoretical formula of the actual potential energy of cracked pillars. In addition, the analytical method of the critical blasting load for cracked pillars is based on the assumption of small internal deformations, ignoring possible plastic deformations. The influence of plastic deformation should be comprehensively considered in future studies. At present, the relevant research on the crack loosen zone width of cracked pillars is limited, with a lack of reasonable engineering sample data. Moreover, measuring errors may be associated with the cracks due to the visibility and the danger of underground operations, which may affect the accuracy of the final calculation results. However, this study focuses on the influence of blasting load on the macro mechanical characteristics of pillars, and analysis based on the visible dominant cracks can essentially reflect the macro stress effect of the pillar.

Conclusions

In the current study, we construct a mechanical model for radial cracked pillars, based on field investigations of a sedimentary bauxite underground mine in Shanxi, China. The mathematical expression of total energy is derived based on the energy dissipation theory. Combined with the instability

Fig. 13 Blasting stress wave velocity monitoring



criterion, the analytical solution of the critical blasting load (q_{cr}) is determined, and the relationship between q_{cr} and pillar height (H), pillar width (b), pillar length (L), and crack loosen zone width (d) is quantitatively investigated.

For a fixed strip pillar length (L) and crack loosen zone width (d), the critical blasting load (q_{cr}) is negatively correlated with pillar height (H). When H and d are fixed, q_{cr} and b are positively correlated. Furthermore, when H and b are constant, q_{cr} gradually increases with L , yet the rate of change is small, indicating that the influence of L is limited. When L and b are fixed, q_{cr} is negatively correlated with d . When the value of d is greater than the inflection point, q_{cr} decreases rapidly. This indicates the serious deterioration of the anti-blasting impact capacity of the pillar.

The numerical simulations reveal that the analytical value of the critical blasting load velocity is less than the maximum value permitted by the Blasting Safety Regulations (GB6722-2014) by approximately 4%. The monitoring results of the

case study indicate that the cracked strip bauxite pillar cannot bear a long-term blasting load beyond the analytical critical value as it reaches a state of over-load instability. In the later period of the monitoring window, both the pillar and the goaf collapse, verifying the rationality of the analytical solution.

Funding This research was supported by the National Natural Science Foundation of China (51974135), the State Key Lab of Subtropical Building Science of South China University of Technology (2020ZB23), the Foundation of Guangdong Key Laboratory of Oceanic Civil Engineering (LMCE202005), and the State Key Research Development Program of China (2016YFC0600802).

Declarations

Conflict of interest The authors declare no competing interests.

References

- Abdellah W, Raju GD, Mitri HS et al (2014) Stability of underground mine development intersections during the life of a mine plan. *Int J Rock Mech Min Sci* 72:173–181
- Agrawal H, Mishra AK (2019) Modified scaled distance regression analysis approach for prediction of blast-induced ground vibration in multi-hole blasting. *J Rock Mech Geotech Eng* 11(01):202–207
- Chen QF, Gu DS, Zhou KP (2012) Catastrophe theory analysis of symmetric cooperative mining artificial pillar instability. *J Central South Univ* 43(6):2338–2342
- Chen Y, Jin Y, Chen M (2015) Rock brittleness evaluation method based on energy dissipation. *J Mech* 47(6):984–993
- Deng J, Kanwar NS, Pandey MD, Xie WC (2019) Dynamic buckling mechanism of pillar rock bursts induced by stress waves. *J Rock Mech Geotech Eng* 11(05):944–953
- Huang QS, Cheng JL, Ding HC et al (2019) Study on the impact of large-scale roof rock collapse impact dynamic load on stope floor failure. *J Min Safety Eng* 36(06):1228–1233 +1239



Fig. 14 Image of collapsed goaf

- Idris MA, Saiang D, Nordlund E (2015) Stochastic assessment of pillar stability at Laisvall mine using Artificial Neural Network. *Tunnel Underground Space Technol* 49:307–319
- Jiang LC, Zeng JJ, Wu AX (2017a) Dynamic response of residual mining excitation based on discrete structure of complex horizontal goaf group. *Chin J Nonferrous Metals* 27(05):1023–1030
- Jiang LC, Zeng JJ, Wu AX (2017b) A quasi-nonlinear vibration model of the dynamic response of horizontal mined-out areas. *J Central South Univ* 48(06):1577–1584
- Kutuzov BN, Tyupin VN (2017) Drilling and blasting design method to ensure preset fragmentation of rocks in open pit mining. *Gornyi Zhurnal* 8:66–69
- Li JT, Wang HW, Lin H (2016) The correlation law of transverse isotropic slate bedding angle and compressive strength and fracture toughness. *J Hunan Univ* 43:126–131
- Li XB, Gong FQ, Wang SF et al (2019) Dynamic and static combined loading mechanical mechanism and dynamic criterion of rock burst in deep hard rock mines. *J Rock Mechan Eng* 38(04):708–723
- Lin WX (2017) Application of shallow hole room and pillar method in underground bauxite mining. *Min Res Dev* 37(12):117–121
- Lu HJ, Liang P, Gan DQ et al (2017) Experimental study on the evolution characteristics of hard rock pillar failure and instability under dynamic disturbance. *J Rock Mechan Eng* 36(S2):3713–3722
- National Standards Compilation Group of the People's Republic of China (2015) *Blasting Safety Regulations (GB6722-2014)*. China Standard Press, Beijing
- Nazarov SA, Specovius-Neugebauer M, Steigemann M (2014) Crack propagation in anisotropic composite structures. *Asymptot Anal* 86(3–4):123–153
- Planinc I, Schnabl S (2019) Analytical buckling loads of columns weakened simultaneously with transverse cracks and partial delamination. *Int J Struct Stab Dyn* 19(3):1950027
- Qin S, Jiao JJ, Wang S (2001) A cusp catastrophe model of instability of slip-buckling slope. *Rock Mech Rock Eng* 34(2):119–134
- Sellers EJ, Klerck P (2000) Modeling of the effect of discontinuities on the extent of the fracture zone surrounding deep tunnels. *Tunnel Underground Space Technol* 15(4):463–469
- Shi YB, Ye YC, Liu YZ, Wang QH, Yue Z, Xia ZQ (2017) Study on the width of strip ore pillar failure based on I-II compound crack failure mode. *J Saf Environ* 17(03):888–895
- Singh R, Sing TN, Dhar DB (1996) Coal pillar loading in shallow mining conditions. *Int J Rock Mech Min Sci Geomech Abstr* 33(8):757–768
- Singh AK, Singh R, Maiti J et al (2011) Assessment of mining induced stress development over coal pillars during depillaring. *Int J Rock Mech Min Sci* 48(5):805–818
- Swift GM, Reddish DJ (2002) Stability problems associated with an abandoned ironstone mine. *Bull Eng Geol Environ* 61:227–239
- Wang ZQ, Li HF (2010) Numerical calculation method and analysis of ore pillar shear safety factor. *J Min Safety Eng* 27(2):277–280
- Xia KZ, Chen CX, Liu XM et al (2017) Rheological mechanics model analysis of gypsum mine pillar-top support system. *Rock Soil Mech* 38(10):2923–2930
- Xu H, Wang YM, Wu AX et al (2017) Calculation model of the thickness of the safe roof thickness of the goaf under the filling body based on the cusp catastrophe theory. *J Rock Mechan Eng* 36(03):579–586
- Yang JX, Liu CY, Yu B, Wu FF (2015a) The effect of a multi-gob, pier-type roof structure on coal pillar load-bearing capacity and stress distribution. *Bull Eng Geol Environ* 74:1267–1273
- Yang YG, Xing LY, Zhang YQ et al (2015b) Research on long-term stability of gypsum pillars based on creep test. *J Rock Mechan Eng* 34(10):2106–2113
- Yin SH, Wu AX, Li XW (2012) Orthogonal range analysis of the sensitivity of factors affecting the stability of the pillar. *J China Coal Soc* 37(S1):48–52
- Yugo N, Shin W (2015) Analysis of blasting damage in adjacent mining excavations. *J Rock Mechan Geotechn Eng* 000(003):282–290
- Zhao K, Yan HB, Feng X et al (2016) Stability analysis of ore pillars based on energy method. *J Mech* 48(04):976–983
- Zhao YS, Feng ZC, Wan ZJ (2003) The principle of minimum energy for rock mass dynamic destruction. *J Rock Mechan Eng* 22(11):1781–1783
- Zhou YY, Feng XT, Xu DP (2016) Experimental study on the mechanical response behavior of thin limestone under bending. *Rock Soil Mech* 37(7):1895–1902
- Zuo JP, Huang YM, Xiong GJ et al (2014) Study on the energy drop coefficient of brittle rock failure. *Rock Soil Mech* 35(2):321–332